Electronic Supplementary Information

Meta-position synergistic effect induced by Ni-Mo co-doping WSe_2 to enhance hydrogen evolution Reaction

Xinya Zhao[a,b], Kankan Liu[*a,b], Fengbo Guo[*a,b], Zeyang He[c], Lixin Zhang[*b,d], Shiwen Lei[e], Huadong Li[a], Yongkang Cheng[a] and Lei Yang[f]

[a] School of Environment and Safety Engineering, North University of China, Taiyuan, 030051, China

[b] Shanxi Key Laboratory of High Performance Battery Materials and Devices, North University of China,Taiyuan, 030051, China

[c] Department of Environment and Geography, University of York, Heslington, York, YO10 5DD, United Kingdom

[d] School of Chemical Engineering and Technology, North University of China, Taiyuan, 030051, China

[e] Institute of coal chemistry, Chinese academy of sciences, Taiyuan, 030000, China

[f] Shenzhen HUASUAN Technology Co.,Ltd, 4168 Liuxian Ave, Nanshan District, Shenzhen, 518055, China

[*]Corresponding authors.

E-mail addresses: liukk@nuc.edu.cn (K. Liu), gfbo@nuc.edu.cn (F.B. Guo), edwardzlx@163.com (L.X. Zhang)

EXPERIMENTAL SECTION

Calculation of the electrochemically active surface area

Capacitance values of the samples can be converted into an electrochemical active surface area (ECSA) using a specific capacitance of flat standard with 1cm^2 of real surface area. By taking the specific capacitance value (C_s) for an ideally flat standard electrode into account, C_s=0.040 mF cm^{-2}, the ECSA can be determined[1, 2]:

$$ECSA = C_{dl}/C_s \quad (1)$$

Calculation of the Turnover Frequency

TOF is calculated as

$$TOF = J * S/(X * F * n) \quad (2)$$

J: current (in A) during the linear sweep measurement.

S: the area of the working electrode.

X: The factor ½ arrives by taking into account that two electrons are required to form one hydrogen.

F: Faraday constant (~ 96485 C mol^{-1}).

n: the number of active sites (mol).

First-Principles Density Functional theory

The free energy of hydrogen adsorption (ΔG_{H*}) is a useful descriptor to describe the activity in acid, ideal hydrogen reduction catalysts have $\Delta G_{H*} \approx 0\ eV$[3]. Hydrogen atom adsorption energy (E_{ad}) is calculated as follows:

$$E_{ad} = E_{M-WSe_2+H} - E_{M-WSe_2} - 0.5E_{H_2} \quad (3)$$

E_{M-WSe_2+H}: the total energy of the catalyst that absorbs one H atom,

E_{M-WSe_2}: the total energy of the catalyst without H atom, where M is Mo, Ni, NiMo,

E_{H_2}: gas phase hydrogen molecular energy.

ΔG_{H*} is calculated as follows:

$$\Delta G_{H*} = E_{ad} + \Delta E_{ZPE} - \Delta TS_H \quad (4)$$

ΔE_{ZPE}: the zero-point energy between the adsorbed hydrogen atom and its reference state in the H_2 molecule.

ΔTS_H: the entropy between the adsorbed H and H_2 molecules in the gas phase.

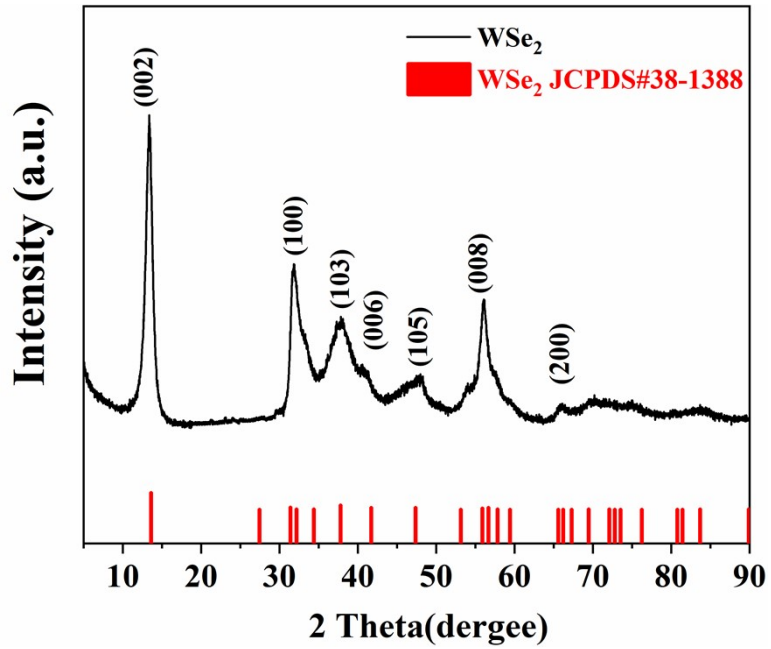

Fig. S1 XRD patterns for WSe_2.

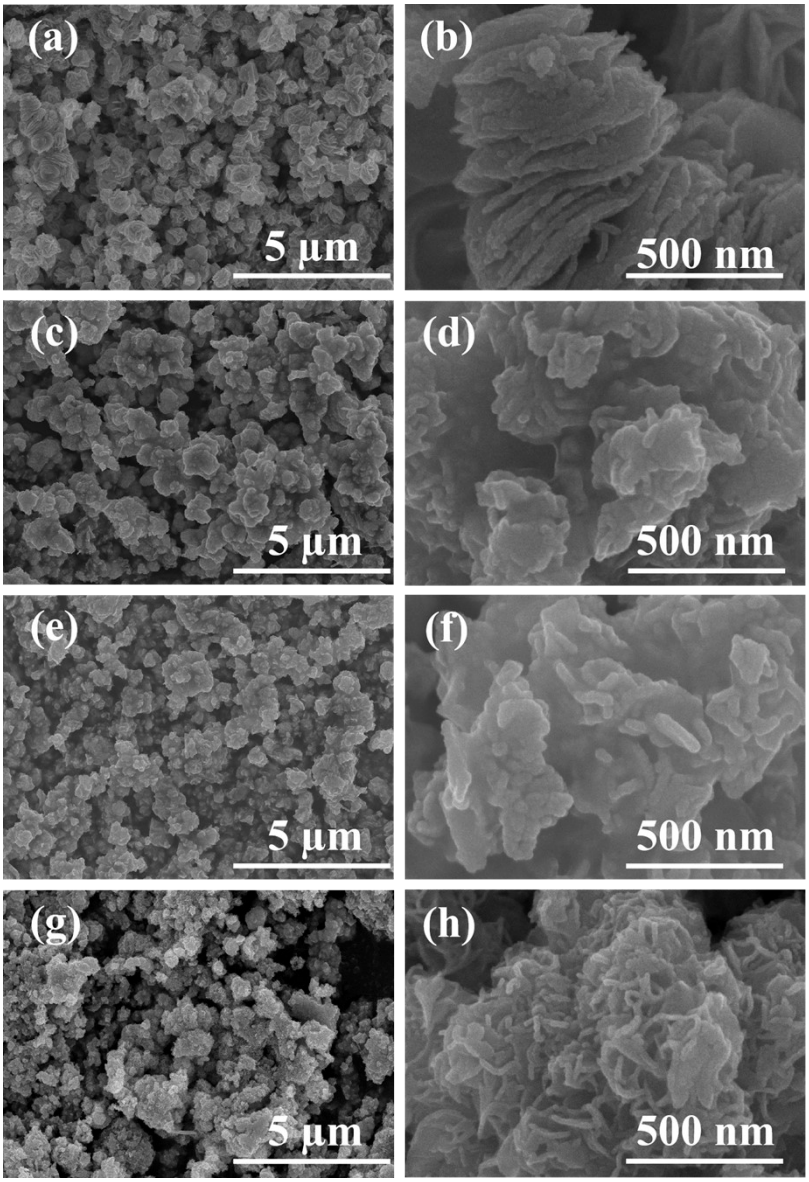

Fig. S2 The different magnifications SEM images of (a, b) WSe_2. (c, d) Mo-WSe_2. (e, f) Ni-WSe_2 and (g, h)NiMo-WSe_2.

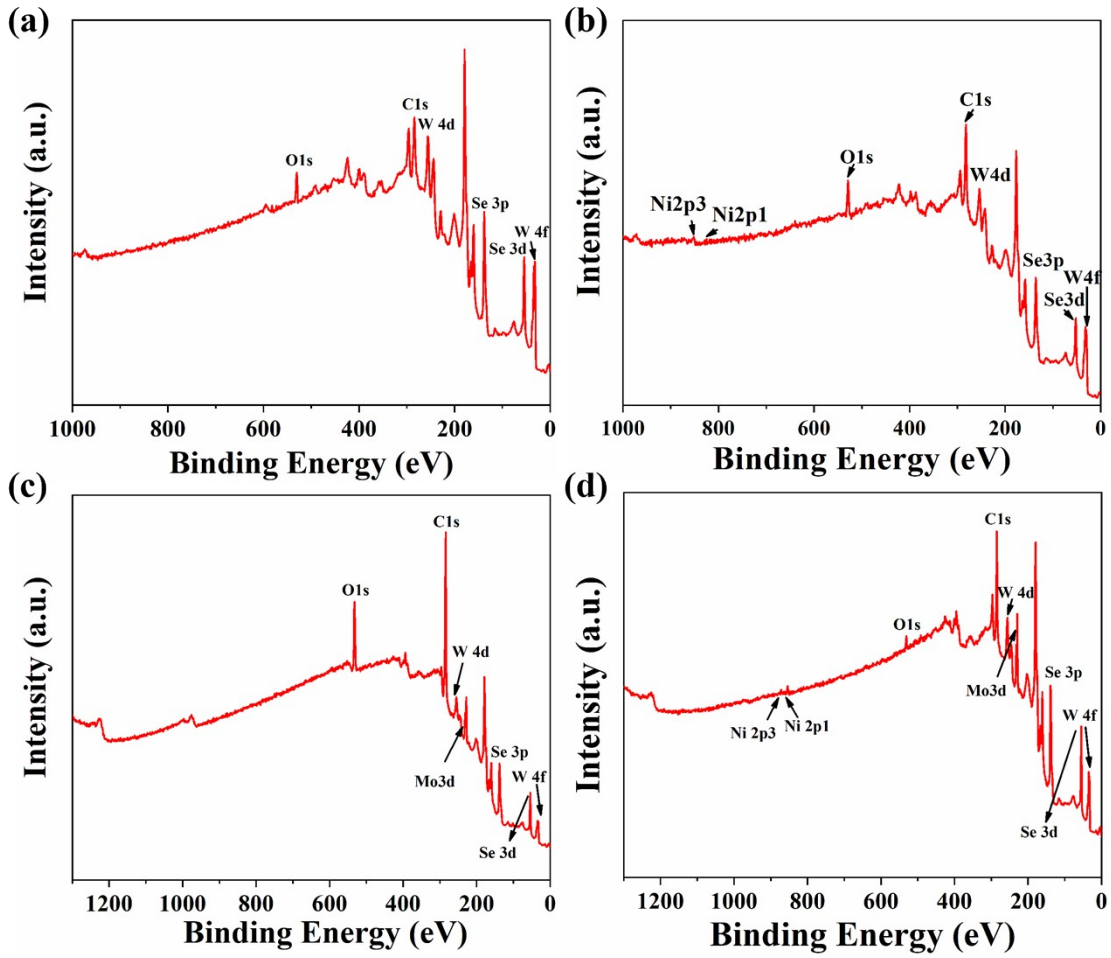

Fig. S3 XPS survey spectra of (a) WSe_2. (b) Mo-WSe_2. (c) Ni-WSe_2 and (d) NiMo-WSe_2.

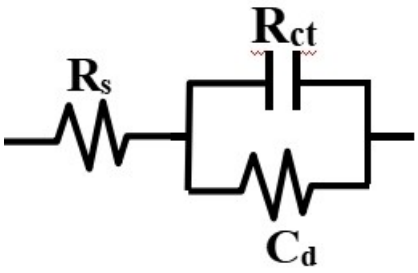

Fig. S4 Equivalent circuit diagram of electrochemical impedance spectroscopy.

Nyquist plot using ZSimDemo software for data fitting, and using an equivalent circuit with a solution resistance (R_s), a charge transfer resistance (R_{ct}), and a constant phase element (C_d). The corresponding diagram of the equivalent circuit is shown in Fig. S4 and the specific simulation results are summarized in Table S6. As displayed in Fig. 5c and Fig. 5h, all Nyquist plots show the similar trends, suggesting that the charge transfer processes and electrochemical mechanisms of the catalysts toward HER are alike, the R_{ct} of the catalyst in 0.5 M H_2SO_4 is less than that in 1 M KOH. It can also be observed that these catalysts have different solution resistances (R_s) in the 0.5 M H_2SO_4 and 1.0 M KOH electrolyte, which are caused by the different contact resistances between electrode and electrolyte. the NiMo-WSe_2 catalyst exhibits the lowest contact resistance in 0.5 M H_2SO_4 and 1 M KOH.

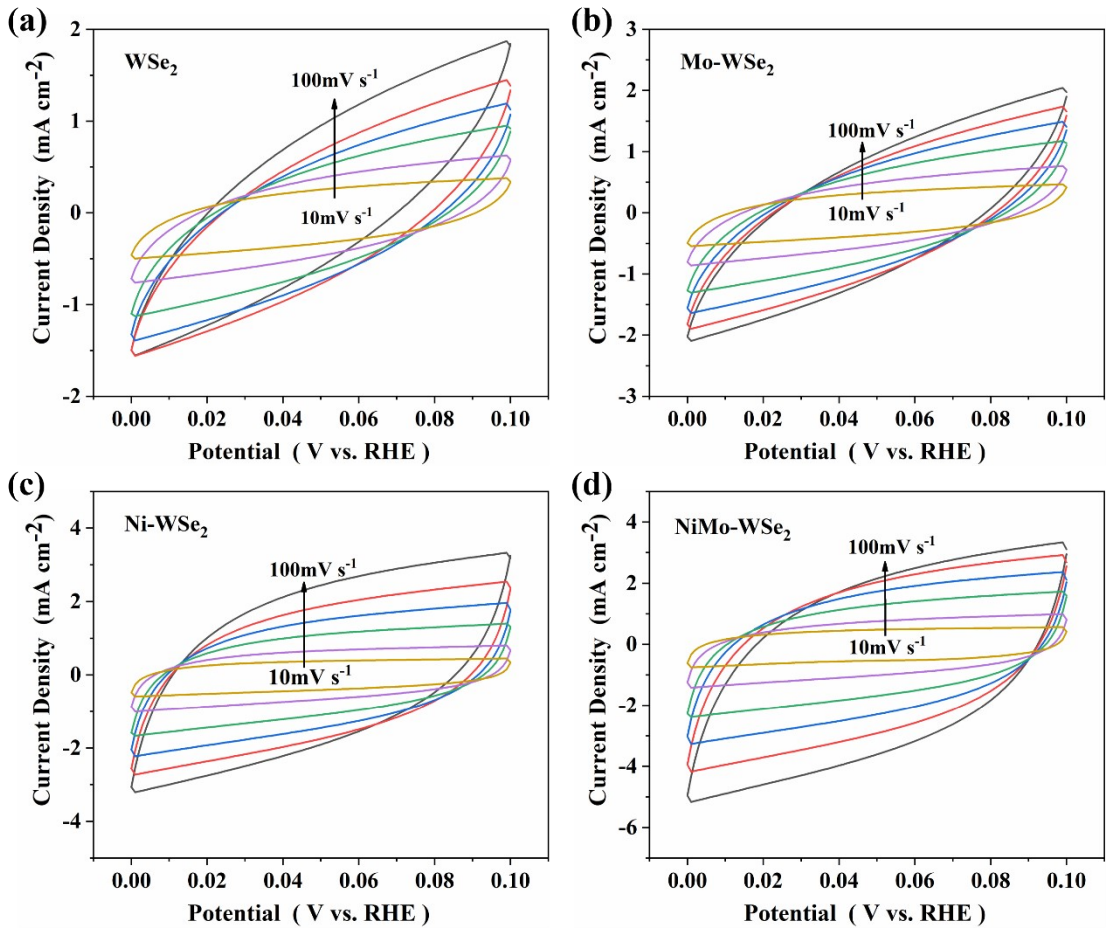

Fig. S5 CV curves in a non-Faradaic potential range (0-0.1 V vs. RHE) of (a) WSe_2. (b) Ni-WSe_2. (c) Mo-WSe_2 and (d) NiMo-WSe_2, in N_2-saturated 0.5 M H_2SO_4 at scan rate of 10 mV s^{-1}, 20 mV s^{-1}, 40 mV s^{-1}, 60 mV s^{-1}, 80 mV s^{-1}, 100 mV s^{-1}.

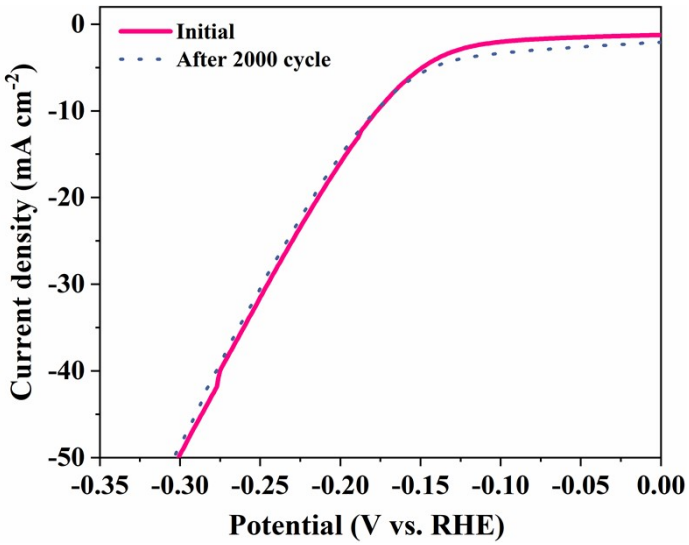

Fig. S6 Stability test of NiMo-WSe_2 sample in 0.5 M H_2SO_4. Polarization curves before (red) and after (blue) continuous 2000 CV cycles.

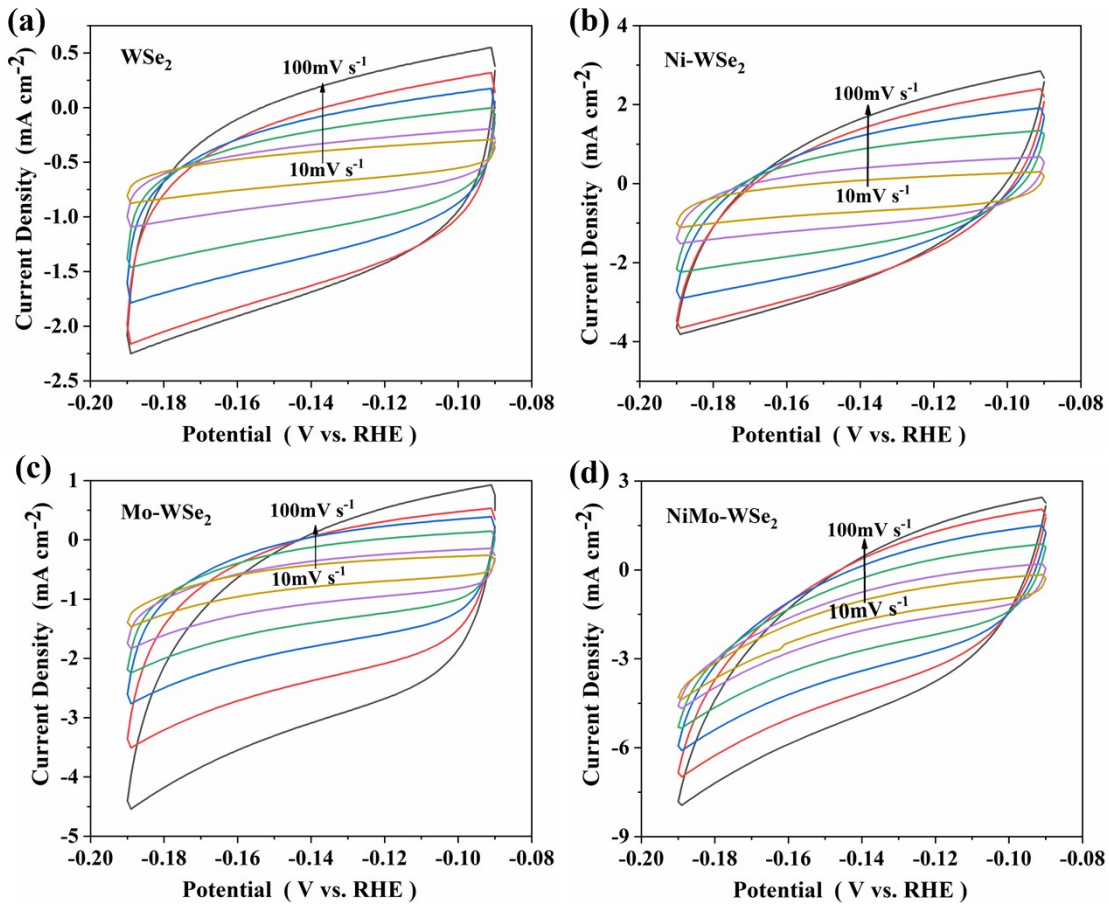

Fig. S7 CV curves in a non-Faradaic potential range (0-0.1 V vs. RHE) of (a) WSe_2. (b) Ni-WSe_2. (c) Mo-WSe_2 and (d) NiMo-WSe_2, in N_2-saturated 1 M KOH at scan rate of 10 mV s^{-1}, 20 mV s^{-1}, 40 mV s^{-1}, 60 mV s^{-1}, 80 mV s^{-1}, 100 mV s^{-1}.

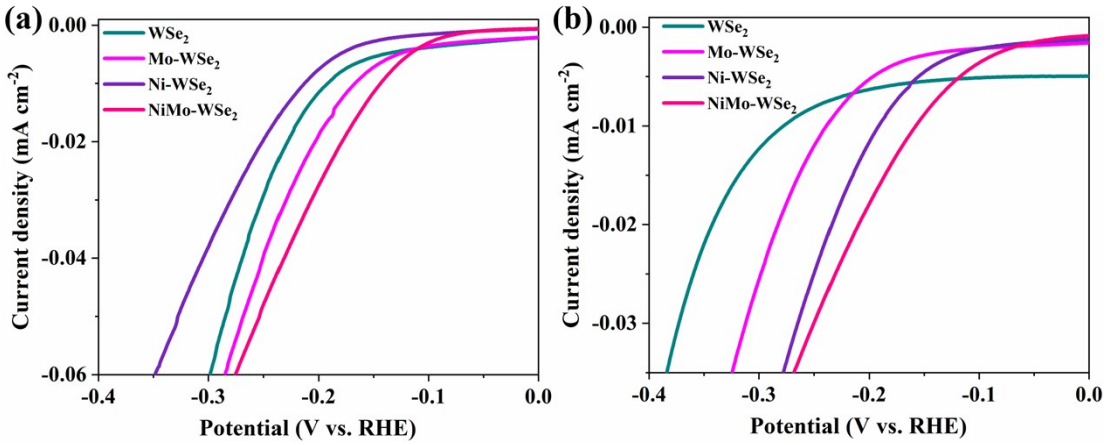

Fig. S8 Polarization curves with the current densities normalized to ECSA in 0.5 M H_2SO_4(a) and 1 M KOH(b) of WSe_2, Mo-WSe_2, Ni-WSe_2 and NiMo-WSe_2.

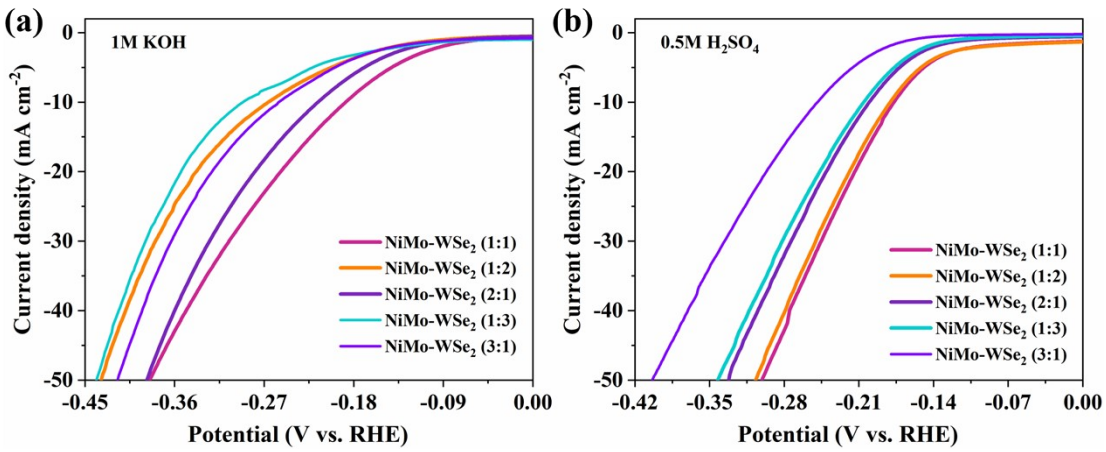

Fig. S9 Polarization curves of NiMo-WSe_2 in 0.5 M H_2SO_4(a) and 1 M KOH(b), where the feed ratio of Ni:Mo is 1:1, 1:2, 2:1, 1:3 and 3:1, respectively.

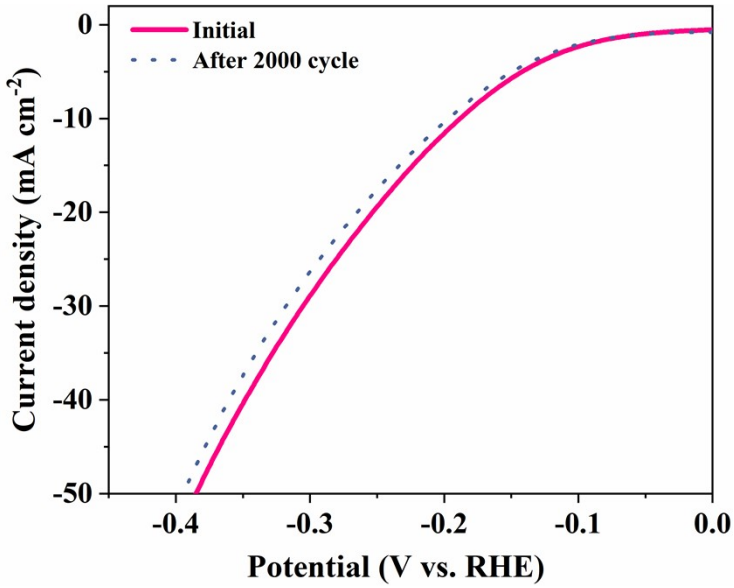

Fig. S10 Stability test of NiMo-WSe_2 sample in 1 M KOH. Polarization curves before (red) and after (blue) continuous 2000 CV cycles.

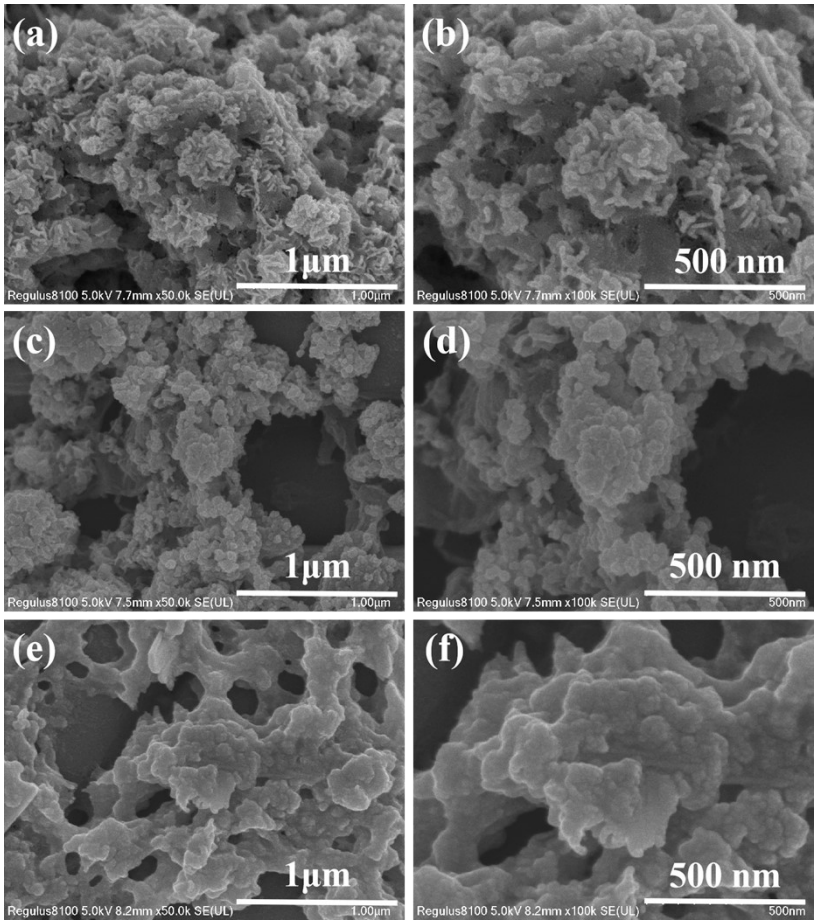

Fig. S11 The different magnifications SEM images of $NiMoWSe_2$ before chronoamperometry (a, b), after 40 h of testing in 0.5 M H_2SO_4 (c, d) and 1 M KOH (e, f).

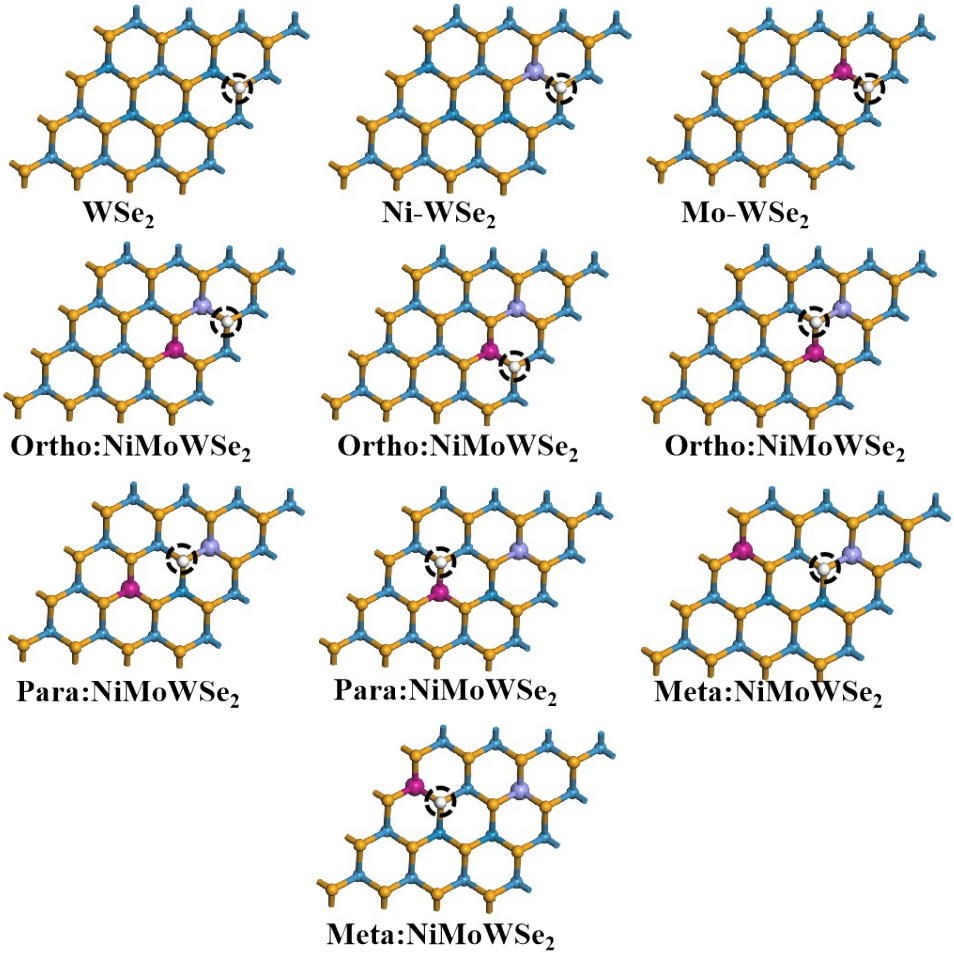

Fig. S12 The top views of the WSe_2, Ni-WSe_2, Mo-WSe_2 and NiMo-WSe_2 model with H^* adsorbed on the varied local configurations.

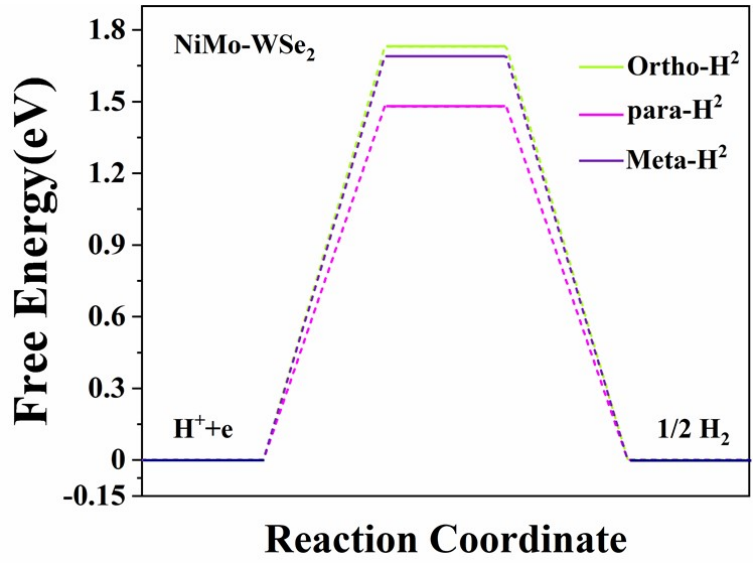

Fig. S13 In NiMo-WSe_2, the hydrogen adsorption point is located at the free energy of Se-Mo when Mo is replaced by Ortho, Para and Meta of Ni for W.

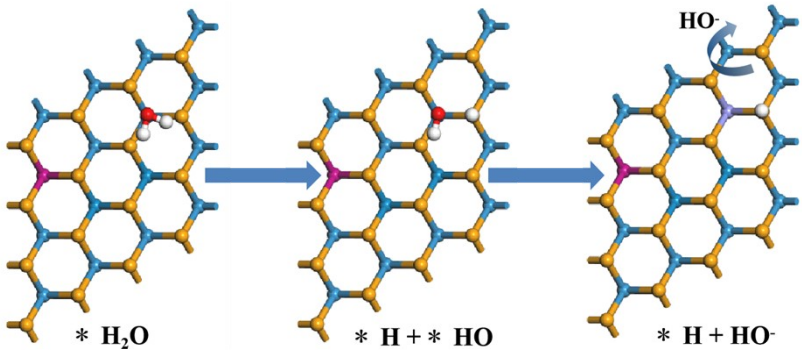

Fig. S14 DFT-optimized geometries of alkaline HER on NiMo-WSe_2(Meta).

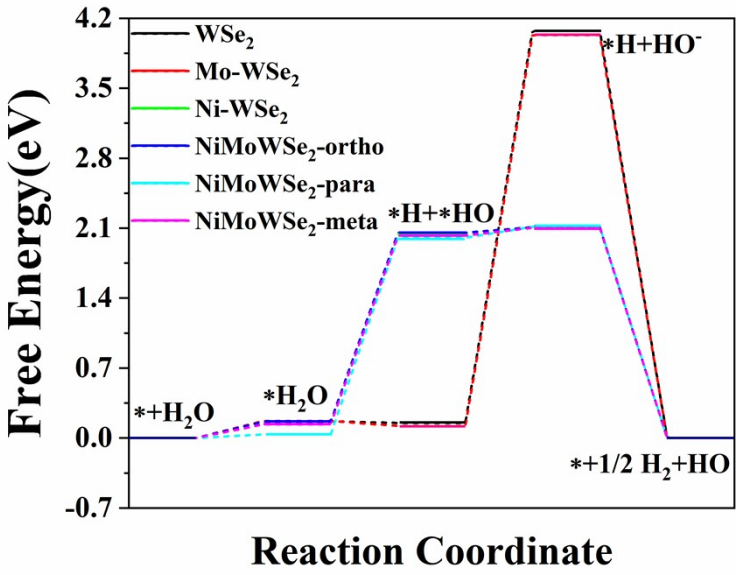

Fig. S15 Free energy diagrams of the WSe_2, Mo-WSe_2, Ni-WSe_2 and NiMo-WSe_2(ortho, para and meta) under alkaline electrolytes.

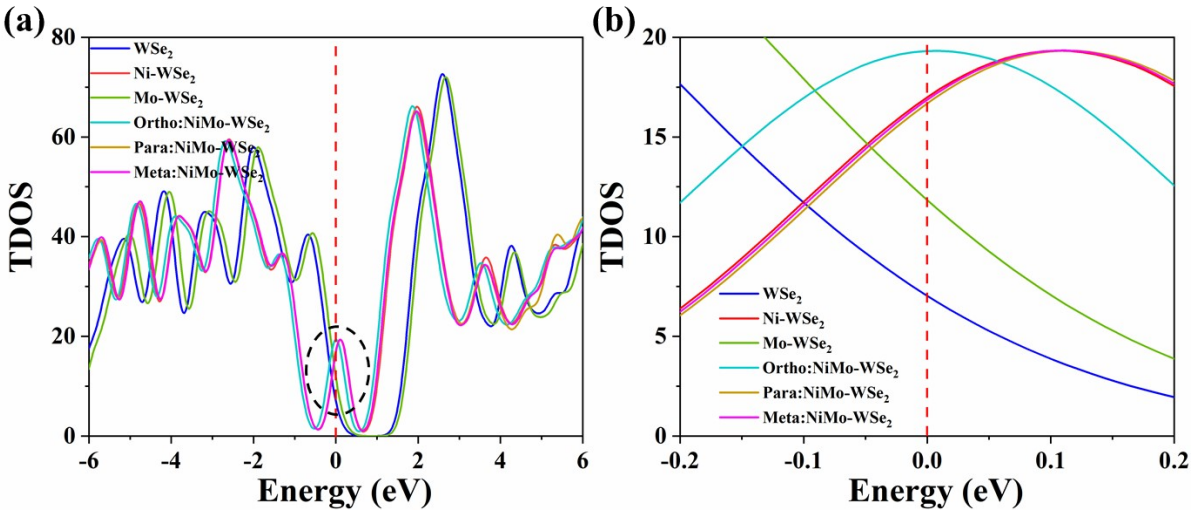

Fig. S16 (a)Total density of states (TDOS) and (b) Partial enlargement for WSe_2, Mo-WSe_2, Ni-WSe_2 and NiMo-WSe_2.

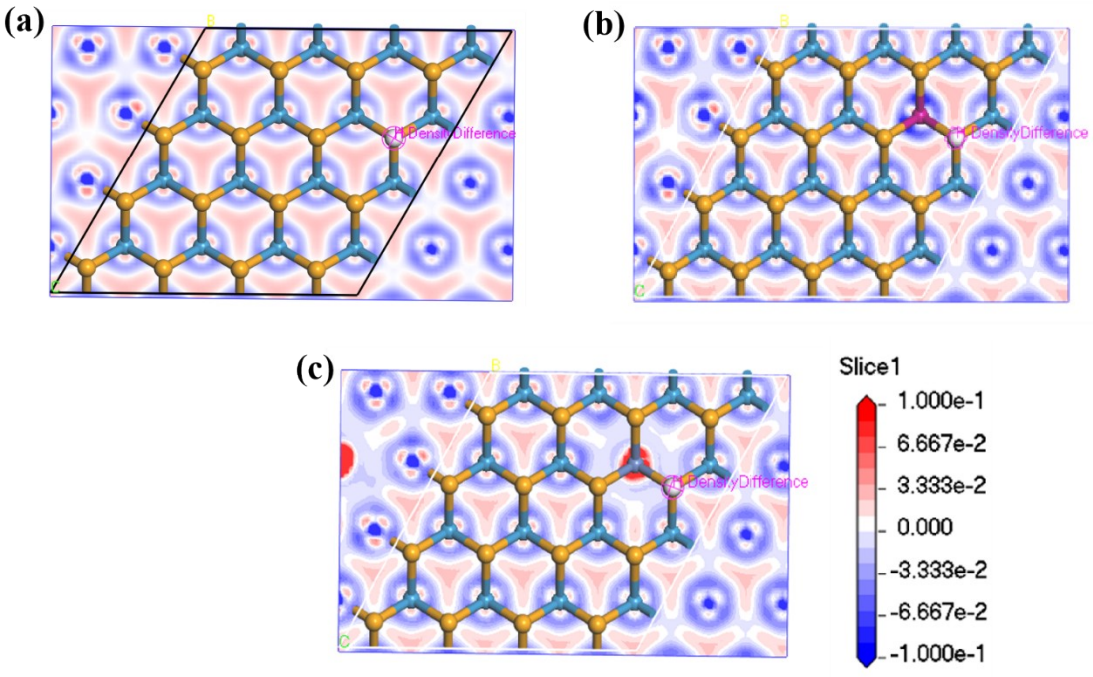

Fig. S17 Charge density difference plot of (a)WSe_2. (b)Mo-WSe_2 and (c)Ni-WSe_2.

Table S1. the specific surface area, Pore volume and Pore diameter.

Sample	Specific surface area ($m^2 g^{-1}$)	Pore volume ($cm^3 g^{-1}$)	Pore diameter (nm)
WSe_2	10.3013	0.061986	20.9762
Mo-WSe_2	23.7397	0.086861	11.6639
Ni-WSe_2	45.1899	0.155643	10.5731
NiMo-WSe_2	47.8663	0.230500	17.3539

Table S2. Peak area obtained for W, Se , Ni, Co and Mo from X-ray photoelectron spectroscopy.

		WSe_2	Mo-WSe_2	Ni-WSe_2	NiMo-WSe_2
W	$4f_{7/2}$	31.56	31.64	31.68	32.61
	$4f_{5/2}$	33.71	33.79	33.84	34.74
	$4f_{7/2}$	35.06	35.24	35.04	35.96
	$4f_{5/2}$	37.17	37.15	37.23	38.22
Se	$3d_{5/2}$	53.79	53.81	53.98	54.79
	$3d_{3/2}$	54.63	54.64	54.80	55.64
Ni	$2p_{3/2}$			853.71	854.17
	$2p_{1/2}$			871.16	871.42
Mo	$3d_{5/2}$		228.15		229.04
	$3d_{3/2}$		231.23		232.15

Table S3. Contents of WSe_2, Mo-WSe_2, Ni-WSe_2 and NiMo-WSe_2 by ICP-AES.

	Ni(at.%)	Mo(at.%)	Se(at.%)	W(at.%)	Atomic ratio of metals (Ni:Mo:Se:W)
WSe_2			67.00	33.00	2.03:1
Mo-WSe_2		4.67	64.02	30.31	1:13.7:6.49
Ni-WSe_2	4.96		65.26	29.78	1:13.16:6.00
NiMo-WSe_2(1:1)	4.83	4.08	65.95	25.14	1:0.84:13.65:5.20

Table S4. Electrochemical HER performance of present work along with previous reports.

Sample	Electrolyte	Over Potential(mV), η at 10 mA cm^{-2}	Tafel slope ($mV\ dec^{-1}$)	Ref.
NiMo-WSe_2	0.5M H_2SO_4	177	82	This work
Mo-WSe_2		279	123	
Ni-WSe_2		249	107	
WSe_2		319	127	
NiMo-WSe_2	1M KOH	188	122	
Mo-WSe_2		303	140	
Ni-WSe_2		240	125	
WSe_2		403	225	
WSe_2	0.5M H_2SO_4	307	126	4
WSe_2	0.5M H_2SO_4	380	105	5
Ni Doped WSe_2		259	86	
Co Doped WSe_2		320	93	
Fe Doped WSe_2		285	85	
Zr Doped WSe_2		322	113	
WSe_2 Nanofilms	0.5M H_2SO_4	239	184	6
RGO/WSe_2	0.5M H_2SO_4	220	57.6	7
Co/hp-WSe_2	0.5M H_2SO_4	268	37	8
WSe_2	0.5M H_2SO_4	353	93	9
Co-WSe_2		225	48	
Co-WSe_2/MWNTs		174	37	
WSe_2–C-20	0.5M H_2SO_4	158	98	10
$Mo_{1-x}W_xSe_2$	0.5M H_2SO_4	209	76	11

Table S5. The fitting specific parameters of EIS spectrum.

	0.5M H_2SO_4		1M KOH	
Catalyst	$R_s(\Omega)$	$R_{ct}(\Omega)$	$R_s(\Omega)$	$R_{ct}(\Omega)$
WSe_2	3.301	26.87	2.739	361.2
Mo-WSe_2	3.607	11.99	2.576	231.8
Ni-WSe_2	2.695	9.782	2.303	189.9
NiMo-WSe_2	2.394	4.177	1.954	23.66

Table S6. TOF value from HER at the overpotential of -0.3V vs RHE for WSe_2, Mo-WSe_2, Ni-WSe_2 and NiMo-WSe_2.

Sample	Current density at -0.3V vs RHE (mV)	n (mol)	TOF
WSe_2	7.815	0.022682579	0.001785
Mo-WSe_2	12.41	0.022848875	0.002814
Ni-WSe_2	19.78	0.022192777	0.004618
NiMo-WSe_2	49.66	0.023165755	0.011108

Table S7. Formation energies (ΔE) for selected different models of WSe_2, Ni-WSe_2, Mo-WSe_2 and NiMo-WSe_2 nanostructures and ΔG_{H^*} value at different hydrogen adsorption sites.

Sample	model	Formation energy ΔE(eV)	Hydrogen adsorption site, H* at the top of Se	ΔG_{H^*}(eV)
WSe_2	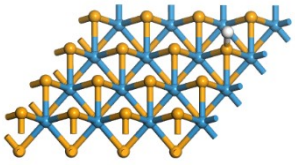	-1.11(per WSe_2)	onto Se–W	2.09
Ni-WSe_2	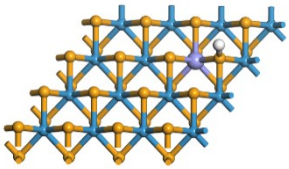	3.72	onto Se–Ni	-0.08
Mo-WSe_2	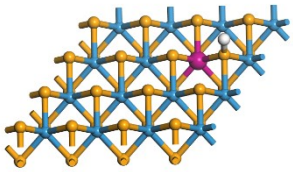	-6.33	onto Se–Mo	2.07
Ortho: NiMo-WSe_2	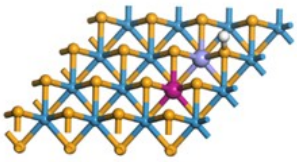		onto Se–Ni	-0.09
Ortho: NiMo-WSe_2	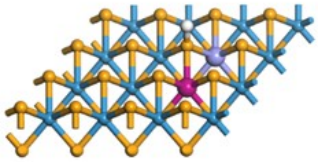	3.46	onto Ni –Se–Mo	-0.1
Ortho: NiMo-WSe_2	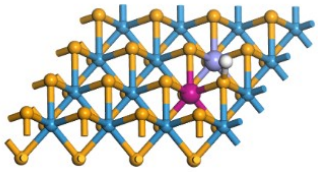		onto Se–Mo	1.73
Para: NiMo-WSe_2	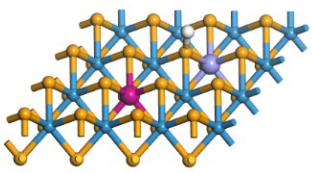	3.39	onto Se–Ni	-0.07

Para: NiMo-WSe_2	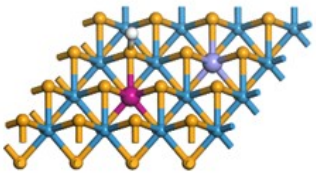	3.48	onto Se–Mo	1.48
Meta: NiMo-WSe_2	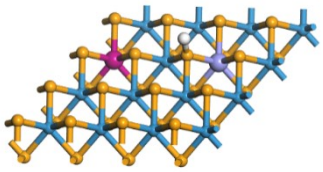		onto Se–Ni	-0.04
Meta: NiMo-WSe_2	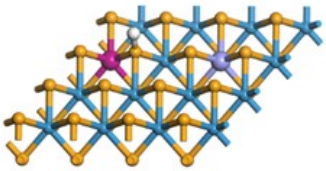		onto Se–Mo	1.69

Table S8. the water dissociation kinetic energy barrier (ΔG_w) of WSe_2, Mo-WSe_2, Ni-WSe_2 and NiMo-WSe_2(ortho, para and meta).

	ΔG_w: $*H_2O \rightarrow *H+*HO$ (eV)	ΔG_w: $*H+*HO \rightarrow *H+HO^-$ (eV)
WSe_2	-0.015	3.925
Mo-WSe_2	-0.051	3.914
Ni-WSe_2	1.887	0.062
NiMo-WSe_2 (Ortho)	1.891	0.056
NiMo-WSe_2 (Para)	1.968	0.109
NiMo-WSe_2 (Meta)	1.890	0.077

Reference

1 M. Zheng, Q. Chen and Q. Zhong, *Dalton Transactions*, 2021, **50**, 13320-13328.

2 D. R. Paudel, U. N. Pan, T. I. Singh, C. C. Gudal, N. H. Kim and J. H. Lee, *Applied Catalysis B-Environmental*, 2021, **286**, 119897.

3 J. Wang, W. Fang, Y. Hu, Y. Zhang, J. Dang, Y. Wu, B. Chen, H. Zhao and Z. Li, *Applied Catalysis B-Environmental*, 2021, **298**, 120490.

4 S. H. Jo, D. H. Kang, J. Shim, J. Jeon, M. H. Jeon, G. Yoo, J. Kim, J. Lee, G. Y. Yeom, S. Lee, H.-Y. Yu, C. Choi and J.-H. Park, *Advanced Materials*, 2016, **28**, 4824-4831.

5 S. R. Kadam, A. N. Enyashin, L. Houben, R. Bar Ziv and M. Bar Sadan, *Journal of Materials Chemistry A*, 2020, **8**, 1403-1416.

6 H. Li, J. Zou, S. Xie, X. Leng, D. Gao, H. Yang and X. Mao, *Journal of Alloys and Compounds*, 2017, **725**, 884-890.

7 X. Wang, Y. Chen, B. Zheng, F. Qi, J. He, P. Li and W. Zhang, *Electrochimica Acta*, 2016, **222**, 1293-1299.

8 Z. Sun, Y. Wang, J. Lang, M. Yang, F. Jin and Y. H. Hu, *Journal of Materials Chemistry A*, 2021, **9**, 13490-13495.

9 G. Zhang, X. Zheng, Q. Xu, J. Zhang, W. Liu and J. Chen, *Journal of Materials Chemistry A*, 2018, **6**, 4793-4800.

10 M. Zou, J. Chen, L. Xiao, H. Zhu, T. Yang, M. Zhang and M. Du, *Journal of Materials Chemistry A*, 2015, **3**, 18090-18097.

11 O. E. Meiron, V. Kuraganti, I. Hod, R. Bar Ziv and M. Bar Sadan, *Nanoscale*, 2017, **9**, 13998-14005.